Criteria for Passive Propellant Control Schemes

H. L. PAYNTER* AND T. R. BARKSDALE†
Martin Marietta Corporation, Denver, Colo.

Experiments were conducted in a drop tower to determine the hydrostatic stability and damping characteristics of perforated plates and screens. The tests were made over a controllable and repeatable acceleration range from 0.0013 to 0.055 g during the 2.1-sec drop interval with three liquids (CH_3OH, CCl_4, and Freon-TF) used to simulate propellants. The acceleration was applied normal to different flat, foraminous barriers in order to settle liquid through the barriers toward the opposite end of the transparent cylindrical tanks. The tests were photographed on Ecktachrome 16 mm film at 200 fps. The Bond Number, Bo, a dimensionless ratio of acceleration-to-capillary forces, was verified as the criterion for predicting hydrostatic stability of the liquid-gas interface at the pores of each barrier. For plates with circular holes, the critical Bo, delineating stability and instability, was 0.84 (based on pore radius). The data tend to support a critical Bo of 0.45, based on one-half the open width, for square-weave screens. Damping results were categorized into seven different regimes and correlated with Weber number, We, a dimensionless ratio of inertia-to-capillary forces.

Nomenclature

A_r = (open area)/(closed area)
a = acceleration
Bo = Bond number
D,d = tube and pore diameters, respectively
f = force
g = gravitational acceleration
h = vertical distance from liquid surface to barrier
K = velocity factor
L = length
m = mass
R = cylindrical tank radius
r = pore radius
w = uncertainty interval
We = Weber number
v = velocity
β = kinematic surface tension, σ/ρ
θ = liquid-to-solid contact angle
μ = absolute viscosity
ρ = mass density
σ = liquid-to-gas-surface tension

Subscripts

Bo = Bond number
c = columnar flow
f,m = force and mass, respectively
R = radius
v,w = vertical travel and wall flow, respectively
ρ,σ = density and surface tension, respectively

Introduction

SURFACE tension device (a screen or perforated plate) can be configured within a propellant tank to orient single-phase fluid at the proper tank outlet (drain or vent) and provide continuous control of the bulk liquid (minimize c.g. offset) in a low-g environment. Ullage pressure supports the liquid in its desired location, while surface tension maintains separation of the fluid phases by stabilizing the liquid-ullage interface at the foraminous material.[1] The simplicity and inherent reliability of these passive systems make them prime candidates for future space missions.[2,3] One such application is for interplanetary spacecraft liquid propulsion systems that require c.g. control and several engine restarts (for course correction, orbit insertion, and orbit trim maneuvers). To provide the desired propellant control, a tank compartmented by means of foraminous barriers is proposed. The location and number of barriers are dictated by the degree of c.g. control required and the number of propellant demands. Liquid is drained from one compartment to the next in the direction favoring the thrust vector; the last compartment is over the tank outlet. The position of the liquid's free-surface at each thrust termination can be above, below, or at the barrier interface. The ability of the foraminous barriers to control and damp propellant motion for these different free-surface conditions under probable force perturbations to the spacecraft is the subject of the present experimental investigation. Drop-tower tests were made under controllable and repeatable accelerations, normal to the material, of 0.0013 to 0.055 g.

Test Apparatus and Procedure

Martin Marietta's 2.1-sec drop tower uses the encapsulated test cell principle.[4] The test cell that houses the experiment, power supply, lights, and camera falls within the 42.0-in.-diam, 116-in.-long drag shield. NEG'ATOR‡ Constant Torque Motors attached to both capsules are used to accelerate the 33.0-in.-diam, 47.0-in.-long test cell downward within the drag shield during the freefall period. The air drag on the test cell and the piston effect due to relative travel between the capsules are both reduced to an insignificant level ($<10^{-5}$ g) by evacuating the drag shield to a pressure of 5.0 mm Hg.

The test setup for both programs is pictured in Fig. 1. The 4.970-in.-i.d. cylindrical glass specimens were 10-in. tall, closed at each end, and contained a perforated barrier positioned 6 in. from the flat bottoms. Before each test the glass specimens were washed in a warm detergent solution, rinsed with tap water, and air-dried. The perforated-plate and screen barriers were dipped in an acid solution, rinsed with water, and air-dried. For the interface stability tests, the specimens were filled with test fluid to a level $\sim\frac{1}{4}$ in. above the upper surface of the foraminous barrier. The test results

Presented as Paper 69-531 at the AIAA 5th Propulsion Joint Specialist Conference, U.S. Air Force Academy, Colo., June 9-13, 1969. This work was performed under Contracts NAS8-20837 and NAS8-21259. L. J. Hastings was Technical Monitor for the George C. Marshall Space Flight Center, Marshall Space Flight Center, Ala.

* Chief, Subsystems Technology Section, Propulsion Research Department. Member AIAA.

† Staff Engineer, Propulsion Research Department.

‡ Tradename, Hunter Spring Co., Hatfield, Pa.

showed that without such a liquid layer, an over-all test setup misalignment, combined with the initial force disturbances present at the start of the drop test, could result in some pores not being covered and produce a hydrodynamic, rather than the desired hydrostatic, pore condition.

The cylindrical specimens were filled to two different liquid levels for the damping tests: 2.0 in. from the bottom surface of the barrier for the lowest applied test acceleration (0.022 g), and 3.0 in. for the two higher accelerations (0.031 and 0.040 g). The corresponding h/R values are 0.806 and 1.205, respectively. The liquid levels were chosen so that the settling liquid would contact the barrier within 1 sec, thereby permitting at least 1 sec to observe damping.

Extreme care was exercised with each test to provide an acceleration normal (within 1° or less) to the barriers. The cylindrical specimens were mounted vertically on a horizontal platform (Fig. 1) that was determined, by means of a transit, to be perpendicular to the vertical centerline of the test cell. The test cell was balanced so that its centerline coincided with a vertical line through its suspension point within the drag shield. The NEG'ATOR spring motors that were used to provide the accelerating force were attached to the bottom of the capsule on this centerline. A plumb bob was used to determine the amount and positioning of balancing weights.

The spring motors were selected on the basis of their constancy-of-force vs linear deflection as determined on a tensile testor (Tinnius Olsen Universal Test Machine). As examples, the three 5-lbf (nominal) motors used for the 0.055-g test condition provided an average force of 16.5 ± 0.25 lbf over their 49 in. deflection range. The single-spring motor, (0.375 lbf nominal) used for the 0.0013-g condition provided an average force of 0.435 ± 0.015 lbf over its 6 in. deflection range.

After assembling the capsule and evacuating the drag shield, the package was hoisted to its 75 ft drop height and allowed to stabilize for 5 min before being dropped. The camera and lights were activated 1 sec before releasing the capsule to permit the camera to attain constant speed (200 fps) and to provide a 1-g reference condition. The transition to the low-g condition is nearly instantaneous (within 15 msec after severing a machine bolt from which the drop package is suspended).

The three test liquids used (methanol, carbon tetrachloride, and Freon-TF, see Table 1), were selected because they exhibited proper physical properties for similitude, the kinematic surface tension β, and the liquid-to-solid contact angle θ. The β range covers both cryogenic and noncryogenic liquid propellants.[6] Propellants are essentially totally-wetting ($\theta \simeq 0°$) to common tank materials such as aluminum, titanium, and stainless steel.[7] Since Pyrex cylinders were used to permit photographic documentation, the test liquids selected had to have $\sigma < 2.67 \times 10^{-3}$ lbf/ft to insure wetting of the cylinders.[8]

Program Results

Interface Stability Tests

Fifty-two barrier configurations, 39 with perforated plate and 13 with square-weave screen, were tested. The plates were of stainless steel and aluminum, and had thicknesses

Table 1 Physical properties of test liquids at zero contact angle and 20°C[5]

Liquid	ρ lbm/ft³	$\sigma \times 10^3$ lbf/ft	$\beta \times 10^4$ ft³/sec²	$\mu \times 10^4$ lbm/ft-sec
CH_3OH	49.4	1.55	10.1	4.02
CCl_4	99.6	1.84	5.95	6.51
Freon-TF	98.6	1.27	4.15	4.70

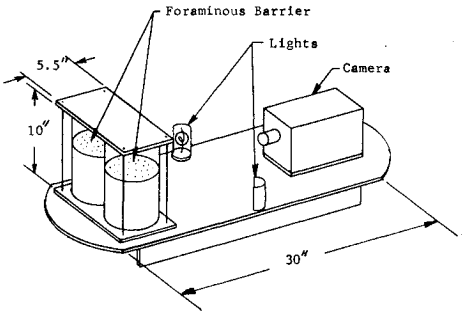

Fig. 1 Test setup.

ranging from 0.018 to 0.190 in. Uniform holes, one diam apart, were positioned on radial circles, and a single hole was drilled at the center of the plate. These holes were first drilled undersize and then reamed to provide a range from 0.281 to 4.562 in. in diameter. The screen barriers were of bronze and stainless steel and had mesh sizes from 1 to 8 (with corresponding pore openings from 0.159 to 0.880 in.).

A barrier was judged to be stable if no gas was ingested through the barrier, or if the liquid-gas interface configuration showed no time dependence after attaining its low-g, minimum-energy shape. The first criterion was used at all acceleration test conditions except the 0.0013-g case. For this case, both the interface configuration and liquid motion up along the wall of the container were used to establish time dependence. Of the two, liquid wall motion could be determined more accurately; if this liquid velocity slowed to zero, the interface configuration was judged as stable. A typical test result for CCl_4 at 0.051 g, after an elapsed drop time of 1.90 sec, is pictured in Fig. 2. The barrier in the left cylinder is stable, but the barrier in the right cylinder is not.

The test data for bare, uncoated, perforated plates are presented in Fig. 3. The pore radii tested are plotted against the ratio of β-to-average test acceleration a. The straight line shown represents $Bo = 0.84$, as calculated from

$$Bo = ar^2/\beta \quad (1)$$

There is some experimental scatter, as shown in Fig. 3, particularly at the lowest acceleration test condition; however, the results verify that Bo is the criterion for hydrostatic pore stability, and provide fairly good agreement with the critical Bo value of 0.84 that separates the stable and unstable regimes. This critical value agrees with earlier analytical work of Bretherton's[9] and previous experimental findings by Hattori[10] for a stable interface in a circular cylinder. As Bretherton pointed out, this value is also obtainable from the Bashforth and Adams tables.[10]

Test results for the screen barriers are presented in Fig. 4. The pore size, as presented, is one-half the open width of the square-weave screen. Again, the data verify the Bo criterion. The critical value of 0.45, based upon one-half the screen opening, is considerably less than that for the plates. Although the acceleration is applied normal to the screen,

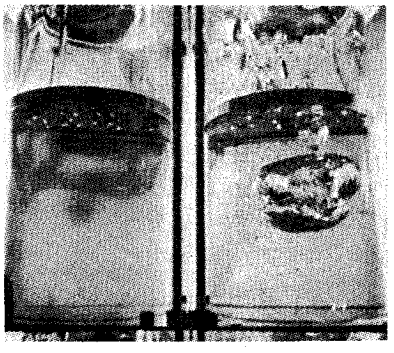

Fig. 2 Typical interface stability results.

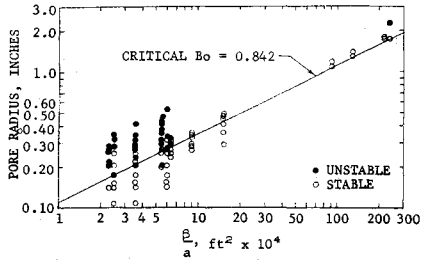

Fig. 3 Stability characteristics for a perforated plate.

the interface stability is reduced by a lateral component of the acceleration as well, due to its complex geometry. The latter results from the fabrication process whereby warp and shute wires are crimped over and under each other. The resultant pore geometry is, therefore, three-dimensional.

The single-sample-experiment technique[12] was used to estimate the accuracy of the Bo determination;

$$w_{Bo} = \left[\left(\frac{\partial Bo}{\partial \sigma} w_\sigma\right)^2 + \left(\frac{\partial Bo}{\partial m} w_m\right)^2 + \left(\frac{\partial Bo}{\partial r} w_r\right)^2 + \left(\frac{\partial Bo}{\partial_f} w_f\right)^2 + \left(\frac{\partial Bo}{\partial \rho} w_\rho\right)^2\right]^{1/2} \quad (2)$$

where w is the uncertainty interval (plus or minus) associated with Bo and the variables in the Bo relationship; and where

$$Bo = \rho f r^2/m\sigma \quad (3)$$

Partially differentiating Bo with respect to each of the variables and nondimensionalizing the second-order uncertainty equation [Eq. (2)] by dividing by the Bo number yields,

$$\frac{w_B}{Bo} = \left[\left(\frac{w_\sigma}{\sigma}\right)^2 + \left(\frac{w_m}{m}\right)^2 + \left(\frac{2w_r}{r}\right)^2 + \left(\frac{w_f}{f}\right)^2 + \left(\frac{w\rho}{\rho}\right)^2\right]^{1/2} \quad (4)$$

Substituting the uncertainty intervals (based upon probable odds of 20:1) for each of the variables provides the following Bo uncertainty limits at the three nominal test conditions: ±6.4% at 0.055 g; ±6.2% at 0.020 g; and ±5.6% at 0.0013 g.

Damping Tests

The following barriers were evaluated:

a) Single perforated plates, 0.032, 0.087, and 0.125 in. thick, with uniform pore diameters ranging from 0.125 to 0.376 in. and A_r's from 0.105 to 0.575; and double-plate specimens comprised of two 0.087-in.-thick aluminum plates, separated by an 0.087-in. gap and skewed so as to provide no open area to flow normal to the flat configuration.

b) Single, stainless-steel, square-weave barriers with mesh sizes of 12 × 12, 30 × 30, 50 × 50, 100 × 100, and 200 × 200 mesh (pore openings of 0.0653, 0.0203, 0.0100, 0.0055, and 0.0029 in., respectively); and double-screen specimens comprised of two 12 × 12 or 30 × 30 mesh screens separated by an 0.087-in. gap.

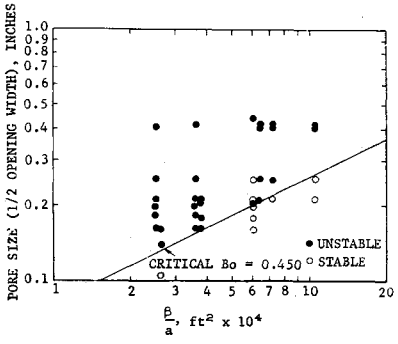

Fig. 4 Stability characteristics for square weave screen.

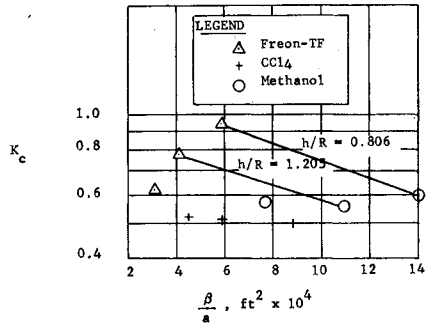

Fig. 5 Column flow velocity.

c) Stainless-steel, Dutch Twill wire cloth, with mesh sizes of 24 × 110, 30 × 250, 165 × 800, 200 × 1400, and 325 × 2300 (pore openings of 0.00551, 0.00276, 0.00138, 0.000709, and 0.000473 in., based upon absolute micron rating, respectively).

d) Multi-tube barriers which consisted of an 0.087 in. aluminum plate with 0.271-in.-i.d. (L/D = 4.4) or 0.183-in.-i.d. (L/D = 4.0) open-ended tubing giving A_r's of 0.178 and 0.143, respectively.

The drop tests were conducted over a settling Bo range from 30.4 to 135.0 at nominal accelerations of 0.022, 0.031, and 0.040 g. The acceleration began with the release of the capsule and acted normal to the flat barriers, tending to settle liquid through the barriers. The settling condition desired for best correlation of test results was that described as regime No. 5.[13] It is characterized by liquid flow along the wall of the cylindrical specimen and also in a single central column. The ability of the barrier to damp the columnar flow was the prime consideration. Wall flow wetted the barrier by capillary action and/or by spreading before column impingement. Tests were also made with a deflector to prevent wall flow from contacting the barrier. The deflector tests permitted evaluation of damping by a nonwetted barrier.

The majority of tests were made without the deflector. For these cases, wall flow always contacted the barrier before impingement of the central liquid column. The wall flow average velocity during settling, v_w, can be described as,

$$v_w = K_w(2aL_v)^{1/2} \quad (5)$$

K_w varied from 0.256 to 0.402, descreasing slightly as a increased, as noted in Table 2. For a given a, $K_w \propto \mu^{-1}$; thus, K_w is greatest for methanol and smallest for CCl_4 (see Table 1).

The maximum impingement velocity for the columnar flow data can be described as

$$v_c = K_c(2ah)^{1/2} \quad (6)$$

where K_c, determined from Fig. 5, varied from 0.495 to 0.601 for methanol and CCl_4 at the two liquid levels (h/R = 0.806 and h/R = 1.205). For Freon-TF, $0.622 \leq K_c \leq 0.945$. The central liquid formation, shape, and flow characteristics were different for the Freon-TF. Following the formation of a central liquid hump, the dome would begin to settle toward the barrier. Subsequent wave phenomena, however, would cause the columnar flow to neck down and

Table 2 Liquid wall flow velocity factors

Liquid	K_w a/g = 0.022	0.031	0.040
CH_3OH	0.402	0.380	0.324
CCl_4	0.318	0.318	0.256
Freon-TF	0.372	0.351	0.304

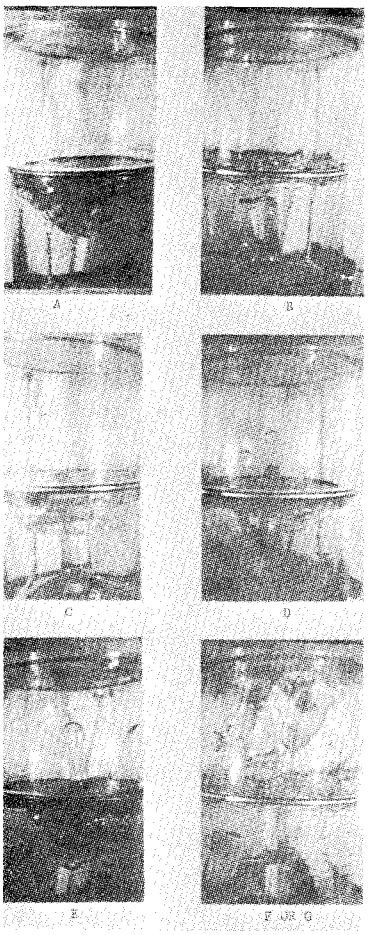

Fig. 6 Damping Categories A through G.

accelerate a smaller diameter dome upward. This motion yielded instantaneous surface accelerations at barrier impact that were greater than those for methanol and CCl_4, particularly at the two lower test accelerations conditions (see Fig. 5).

A film analyzer and recorder (Boscar Model N-1) was used to measure displacement of wall flow and columnar flow as a function of test time. A single film frame was projected on a 20 × 20 in. screen containing a set of movable cross wires. Movement was translated into coded signals that were stored and displayed digitally on command. A movement of 0.002 in. was one machine count. A vertical scale, photographed with each test, was used to calibrate the machine readings. The latter, in 1 in. increments from the initial liquid level to the barrier, were determined before measuring the displacement. The test interval was determined by film frame count and timing pips (20/sec) on the film. Velocity data were obtained by graphical differentiation of the flow histories.

Damping performance was categorized by the following regimes (Fig. 6): a) no liquid passes through the barrier, b) some liquid (relatively little) passes during wetting of the barrier by liquid settling along the wall of the cylindrical specimen, c) The dome of the liquid column either penetrates the barrier, resulting in a sessile globule, or recedes completely, d) the central liquid mass penetrates the barrier as one or two columns that pinch off and stay above the barrier, but no additional liquid passes, e) similar to D but the columns are not completely pinched off, f) a considerable amount of liquid passes through most of the barrier surface, and there are a number of columns (streamers), and g) a massive amount of liquid passes through the barrier with no apparent damping.

Regime A is most desired; B and C also show good damping. Regimes F and G display negligible damping. Categories D and E separate the damped and undamped regimes (Fig. 6).

The damping performance of each barrier was correlated with the impingement Weber number, We, at the pores of the barrier using the relationship

$$We = v_c^2 r/\beta \tag{7}$$

The pore radii (r) for perforated-plate and square-weave barriers are one-half the open-pore dimension; but for Dutch Twill, an effective radius of one-half the pore openings (based on absolute micron rating) was used.

The damping performance for the single- and double-perforated-plate and the single-square-weave and Dutch-Twill-screen barriers is presented in Fig. 7. The single-plate and square-weave results are for an initially-wet screen only (tests with no wall-flow deflector). Some liquid (category B) always passed through the single plate and single and double square-weave screens during the initial barrier wetting. The double-plate and Dutch Twill results are given for both initially-wetted and nonwetted barriers, since the initial barrier condition had no noticeable effect on damping performance. This was not the case for the other barriers.

The single-plate results shown in Fig. 7 are for $A_r \leq 0.176$. Poor damping categories F and G were observed for all tests made at two higher A_r's, 0.430 and 0.575. A drastic per formance difference was also observed between an initially-

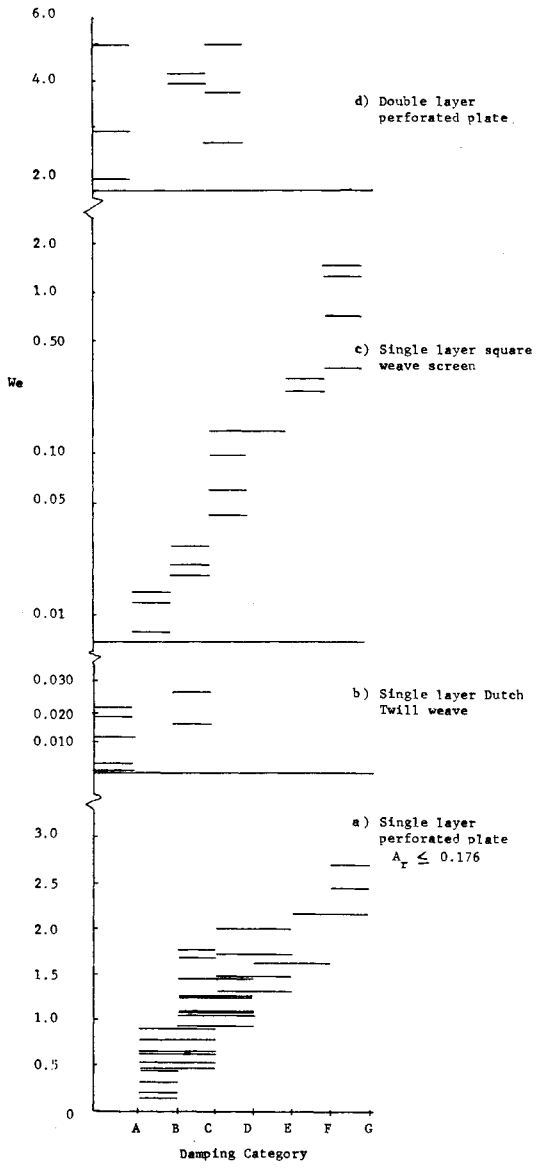

Fig. 7 Barrier damping performance.

nonwetted and a wetted barrier. For example, the same barrier that showed category B damping at $We = 0.626$ (initially-wet) displayed category E damping at $We = 0.463$ (initially nonwetted). Similarly, another barrier showed category C damping at $We = 1.691$, but category F damping at a lower We number ($We = 0.806$).

The Dutch Twill screen displayed category A damping for most tests. The small pore radii resulted in relatively low We numbers. It is interesting to note that the category C damping observed at $We = 0.018$ compares to that for the square-weave screen. The damping performance of the double-layer square-weave barriers was comparable to that for the single square-weave screen.

The double-plate and Dutch Twill barriers performed best. These differ from the other barriers in that neither affords an open area to the settled liquid flow. Rather, they cause the flow to take a tortuous path through the barrier, but at the same time provide a capillary network to inhibit and maintain wetting; both factors are pertinent to good damping performance.

There was no apparent effect of plate thickness on barrier performance for the thicknesses tested (including those for the multi-tube barriers with the tubes flush with the bottom of the plate). The performance results for the multi-tube configuration, in which the tubes protruded below the plate, were comparable to those for the single-perforated-plate barriers.

The method for single-sample experiments[12] was used to provide some measure of reliability of test results. Following the manner discussed earlier, the uncertainty limits (based on the cylinder radius R) at the three nominal low-g test conditions yielded for the settling Bo: $\pm 5.5\%$ at 0.040 g; $\pm 5.8\%$ at 0.031 g; and $\pm 6.5\%$ at 0.022 g. The impingement We uncertainty limit is estimated to be less than $\pm 10.8\%$.

Concluding Remarks

The test results are applicable to the design of surface tension systems when considering pore stability and damping characteristics under a constant acceleration acting normal to the foraminous surface. A particular design condition is that following an engine burn. During such a burn, a favorable acceleration vector is generated that tends to position and maintain propellant at the tank outlet. Following engine shutdown, the vehicle is exposed to a low-level force (drag) that tends to settle propellant away from the outlet. If the propellant level is above, or at, the foraminous barrier, the Bond number (Bo) stability criteria presented in this paper are applicable. For the first condition, propellant above the barrier will settle away from the barrier and expose the liquid-ullage interface condition at the pores of the barrier. This, then, becomes the second condition that was investigated during this program. The critical Bo values are 0.450 and 0.842 for square-weave screen and perforated plate, respectively.

If the propellant level is below the foraminous barrier following the engine shutdown, the damping results presented in this paper are applicable, provided that: 1) the tank is cylindrical, 2) the settling acceleration a is axisymmetric and normal to the barrier, 3) the free surface of the propellant is flat ($Bo \gg 1000$) following engine shutdown, 4) the settling Bo is between 30.4 and 135, and 5) the nondimensional vertical distance ($h \div$ tank radius R) from the liquid to the barrier is less than the h/R values presented here. If these conditions are satisfied, the designer may use the K_c factor from Fig. 5 to calculate the maximum impingement velocity. (The velocity will be conservative, since $a \propto R^2$ for a given Bo, while the liquid travel distance h is scaled linearly with h/R.) He then may determine the type of barrier configuration and pore size needed to provide the desired damping as a function of the impingement Weber number (calculable with the impingement velocity, pore size, and liquid propellant properties). The barrier configurations recommended for consideration, based on performance measured during this program, are the double-perforated-plate and Dutch Twill barriers.

References

[1] Bowman, T. E. and Paynter, H. L., "Weightless Liquids," *Science Journal*, Vol. 2, No. 9, London, Sept. 1966, pp. 44–49.

[2] Morgan, L. L. et al., "Orbital Refueling and Checkout Study: Conceptual Designs of Fluid Transfer Systems," Final Report, Feb. 1968, Tl-51-67-21, Vol. 5, Lockheed Missiles & Space Co., Sunnyvale, Calif.

[3] Balzer, D. L. et al., "Advanced Propellant Management System for Spacecraft Propulsion Systems, Phase I—Survey Study and Evaluation," MCR-69-87, Feb. 1969, Martin Marietta Corp., Denver, Colo.

[4] Paynter, H. L., "The Martin Company's Low-g Experimental Facility," *Proceedings of the Symposium on Fluid Mechanics and Heat Transfer Under Low Gravity*, United States Air Force Office of Scientific Research and Lockheed Missiles and Space Company, June 1965, pp. 15–1 to 15–17.

[5] Salzman, J. A. et al., "An Experimental Investigation of the Frequency and Viscous Damping of Liquids During Weightlessness," TN-D-4132, Aug. 1967, NASA.

[6] Barksdale, T. R. and Paynter, H. L., "Design, Fabrication, and Testing of Subscale Propellant Tanks with Capillary Traps," MCR-68-11, March 1968, Martin Marietta Corp., Denver, Colo.

[7] Lyerly, G. A. and Peper, H., "Summary Report—Studies of Interfacial Surface Energies," NASA-CR-54175, Dec. 1964, Harris Research Labs., Washington, D.C.

[8] Zisman, W. A., "Relation of Equilibrium Contact Angle to Liquid and Solid Constitution," *Proceedings of the Symposium on Contact Angle, Wettability, and Adhesion*, Advances in Chemistry Series No. 43, American Chemical Society, 1964, p. 20.

[9] Bretherton, F. P., "The Motion of Bubbles in Long Tubes," *Journal of Fluid Mechanics*, Vol. 10, 1961, pp. 166–188.

[10] Hattori, S., "On the Motion of a Cylindrical Bubble in a Tube and its Application to the Measurement of the Surface Tension of a Liquid," Rept. 115, 1935, Aeronautical Research Institute, Tokyo Imperial Univ., Tokyo, Japan.

[11] Bashforth, F. and Adams, J. C., *An Attempt to Test the Theories of Capillary Action*, University Press, Cambridge, England, 1883.

[12] Kline, S. J. and McClintock, F. A., "Describing Uncertainties in Single-Sample Experiments," *Mechanical Engineering*, Jan. 1953, pp. 3–8.

[13] Bowman, T. E., "Cryogenic Liquid Experiments in Orbit: Liquid Settling and Interface Dynamics," NASA-CR-651, Dec. 1966, Vol. 1, Martin Marietta Corp., Denver, Col.